IEEE Access
Multidisciplinary | Rapid Review | Open Access Journal

Received 19 December 2022, accepted 3 January 2023, date of publication 5 January 2023, date of current version 11 January 2023.

Digital Object Identifier 10.1109/ACCESS.2023.3234614

RESEARCH ARTICLE

A Method for Predicting the Boring Topography Error of Shaft Hole on a Thin-Walled Box Based on a Proposed Dynamic Model

DINGQIANG PENG, LANTAO YANG, AND YIMIN SHAO
State Key Laboratory of Mechanical Transmission, Chongqing University, Chongqing 400044, China
College of Mechanical and Vehicle Engineering, Chongqing University, Chongqing 400044, China

Corresponding author: Lantao Yang (ltyang@cqu.edu.cn)

This work was supported by the National Natural Science Foundation of China under Grant 52035002 and Grant 51475053.

ABSTRACT Traditional boring dynamic model ignores the effect of the uneven radial stiffness of the shaft hole of the thin-walled box on the boring vibration characteristic, which will lead to the deviation in the prediction for both the cutting force and the surface topography of the machining hole. To address this shortcoming, a new calculation model of the equivalent radial stiffness of the shaft hole is proposed and then validated by the finite element (FE) method. On this basis, a boring dynamic model of the shaft hole is developed, and an experimental study on the dynamic characteristics of the shaft hole boring is carried out to verify the correctness and effectiveness of the proposed dynamic model. Moreover, a prediction method for the surface topography error of the machined shaft hole is presented based on the proposed dynamic model. Finally, the comparison investigation on the hole machined surface topography predicted by the proposed method and measured in practice is carried out. The results show that the proposed theoretical models and method can achieve accurate predictions for both the boring cutting force and the machined surface topography error of the shaft hole on the thin-walled box. This study can provide a theoretical basis for machining error control and process optimization of the fine boring of the thin-walled transmission box.

INDEX TERMS Thin-walled box, shaft hole machining, boring dynamic model, surface topography prediction.

I. INTRODUCTION

High-power density transmission box system has the advantages of compact structure, and precise and efficient transmission, which is widely used in the transmission equipment of vehicles, ships and aviation [1], [2], [3]. However, it is easy to deform or vibrate in processing due to the box-shaped part structure with lower stiffness. Thus, the machining accuracy of the transmission box shaft hole is difficult to control [4]. As a key feature of the transmission box, the machined surface topography error of the shaft hole directly determines the assembly accuracy of the transmission components and is closely related to the dynamic service performance of the whole box. The boring dynamic model is an important theoretical means to study the dynamic behavior of shaft hole machining and to develop prediction methods for the shaft hole machined surface topography error. To establish the boring dynamic model is the benefit to understand the forming mechanism of machining error, and be timely controlled to avoid unexpected phenomena occurrence, but how to improve its calculation accuracy is a prerequisite for predicting the cutting force and the surface topography of the shaft hole [5].

The fluctuation of cutting force can lead to the vibration of the cutter and workpiece, and then affect the machining precision of the workpiece in process. Accurately modelling cutting force has become an important theoretical means for scholars to establish the prediction of machining surface topography error and evaluate the cutting stability [6], [7], [8]. For example, Sabberwal et al. [9] were the first to demonstrate that the cutting force is proportional to the chip load area, and the proportionality coefficient depends on the workpiece and cutter material characteristics and cutting

The associate editor coordinating the review of this manuscript and approving it for publication was Giambattista Gruosso.

conditions. Subramani et al. [10] proposed a simple analytical model for calculating the cutting force of boring. In their model, the cutting force components were obtained by using an equivalent chip flow angle. Based on the work in [10], Kuster et al. [11] carried out a cutting dynamic model by considering the regenerative chatter. Then, Atabey et al. [12] developed two models to predict the cutting force during the boring process. Young et al. [13] proposed a model for predicting the cutting force, in which the equivalent cutting edge was defined and used. Later, Wang et al. [14] improved their model by considering the influences of inclination and rake angles. The cutting force depends heavily on the dynamic parameters of the cutting system and can be obtained from the dynamic model of the machining system.

Establishing the dynamic model of the machining system is a basic theoretical method to evaluate the mechanical properties of machining and predict the precision of the machined surface topography, which plays an important role in industrial practices [15]. In recent years, scholars have paid more and more attention to the dynamic modelling of machining systems [16]. For example, Lazoglu et al. [16] proposed a time-domain mathematical model for solving the dynamics in the boring process and then studied the influence of boring parameters on cutting force. Ozlu et al. [17] developed a discretization method of the trapezoidal differential element to calculate the cutting area and cutting force, and then to observe the impact of tool nose radius on machining stability. Moetakef-Imani et al. [18] used the Euler-Bernoulli beam theory to conduct dynamic modelling of the boring bar. Miguelez et al. [19] established a dynamic model to study the flutter suppression performance of a boring bar. Ghorbani et al. [20] evaluated the vibration characteristics of the boring bar by changing its dynamic parameters. Chockalingam et al. [21] established a model to study the damping capacity and flutter performance of the boring tool. Fallah et al. [22] proposed a chatter vibration mechanical model of the boring bar to simulate the nonlinear dynamic characteristics of the forward path.

In the current boring dynamic modelling, the influence of the radial stiffness of the cutter rod on the dynamic behavior of the boring system is focused. However, the thin wall with the shaft hole attached is prone to a large deformation in the boring process, which will lead to a large difference in the radial stiffness of the shaft hole in different directions, and then affect the dynamic characteristics of the boring system. While this effect can not be considered in the traditional dynamic model of the boring system, which is bound to lead to a large deviation in the prediction for both the boring dynamic behavior and machining topography error.

Therefore, given the problems mentioned above, the main contributions and highlights of this paper are summarized as follows:

- A new analytical calculation model of the radial stiffness of the shaft hole on the thin-walled box is established, and its accuracy is validated by the FE method.
- A dynamic model of the boring system is proposed by considering the supporting deformation of the shaft hole, and its correctness and effectiveness are validated by conducting an experimental study.
- Combined with the established dynamic model, a prediction method for the surface topography error of the boring shaft hole is developed, and its prediction effect is proved by actual measured results.

The following structure of this paper is arranged as follows: The problem that needs to be addressed in this paper is introduced in Section II. The proposed shaft hole radial stiffness calculation model and boring dynamic model are demonstrated in Section III. The established shaft hole radial stiffness verification FE model and the verification experiment of the boring dynamic characteristics are presented in Section IV. Then the proposed prediction method for the surface topography error of the machined shaft hole is described in Section V. In addition, the results obtained from the proposed models and method are analyzed and discussed in Section VI. Finally, some main conclusions are drawn in Section VII.

II. PROBLEM FORMULATION

The force analysis of the boring system is shown in Fig. 1 (a). The complex time-varying cutting force is generated due to the extrusion motion of the insert and the hole wall. The cutting force is decomposed into three mutually perpendicular components, namely F_f, F_r and F_t, along the axial, radial and tangential directions of the boring rod.

Fig. 1 (b) shows the error generation process analysis during the boring process. The point O_N is the fixed reference point of the relative machine coordinate system {G}. On the plane XYO_N, the boring cutter is deflected by the radial force F_{cr} and tangential force F_{ct}, which makes the center point O_C of the boring bar deviate from the position O_N and form the displacement e_c. According to the third law of Newton mechanics, there are equivalent inverse forces F_{hr} and F_{ht} acting on the hole wall to cause additional deformation of the box wall, which makes the center point O_H of the shaft hole away from the position O_N and then the offset e_h occurs. The offset e_c and e_h together constrain the change of instantaneous chip thickness in the boring process.

Combining with Fig. 1 (a) and (b), the transformation relation of cutting component forces in two coordinate forms that describe box wall deformation by cartesian coordinates and boring bar deflection by polar coordinates, is established, namely:

$$\begin{bmatrix} F_{hx} \\ F_{hy} \\ F_{hz} \end{bmatrix} = \begin{bmatrix} \cos\theta & \cos(\theta - \pi/2) & 0 \\ \sin\theta & \sin(\theta - \pi/2) & 0 \\ 0 & 0 & -1 \end{bmatrix} \cdot \begin{bmatrix} F_{hr} \\ F_{ht} \\ F_{hf} \end{bmatrix} \quad (1)$$

Fig. 2 shows the simplified cantilever beam model of the shaft hole on the thin-walled box. In Fig. 2, points A and B denote ectopic two points on the circumference of the shaft hole and point C refers to the endpoint of the shaft hole attached to the thin wall. Since the shaft hole is contained in

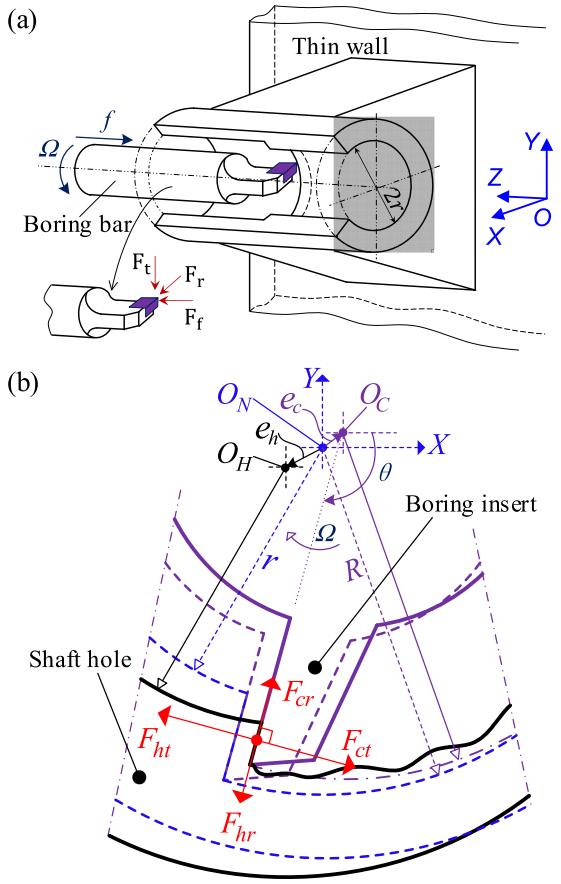

FIGURE 1. Force analysis of the boring system: (a) boring processing schematic; (b) topography error formation analysis.

the suspended beam structure, it is assumed that the component of the cutting force in the X direction is always collinear with point C, thus the bending moment of this component on point C equals zero. Therefore, when the cutting force acts at points A and B, the bending moment of point C is,

$$\begin{cases} M_A^C = F_{hy}^A \cdot l_A \\ M_B^C = F_{hy}^B \cdot l_B \end{cases} \tag{2}$$

Assuming that the bending strength of the box wall at point C is I_C, $F_{hx}^{\mathrm{A}} = F_{hx}^{\mathrm{B}}$ and $F_{hy}^{\mathrm{A}} = F_{hy}^{\mathrm{B}}$. Since $l_{\mathrm{A}} < l_{\mathrm{B}}$, then $|M_A^C| < |M_B^C|$. The angle of the wall-attached suspension beam caused by M_A^C and M_B^C refers to ϕ_A^C and ϕ_B^C, respectively. Thus there is $\phi_A^C < \phi_B^C$. In these two cases, the offset of the hole axis point O_H can be expressed as,

$$\begin{cases} \Delta x_{i\varphi} = \varphi_i^C \cdot L \cdot \sin\left(\varphi_i^C\right) \\ \Delta y_{i\varphi} = \varphi_i^C \cdot L \cdot \cos\left(\varphi_i^C\right) \end{cases} \tag{3}$$

The equivalent directional stiffness of points A and B relative to the hole center O_H can be expressed as,

$$\begin{cases} k_{hx}^{ie} = \dfrac{F_{hx}^i}{\Delta x_{i\varphi} + \Delta x_C} \\ k_{hy}^{ie} = \dfrac{F_{hy}^i}{\Delta y_{i\varphi} + \Delta y_C} \end{cases} \tag{4}$$

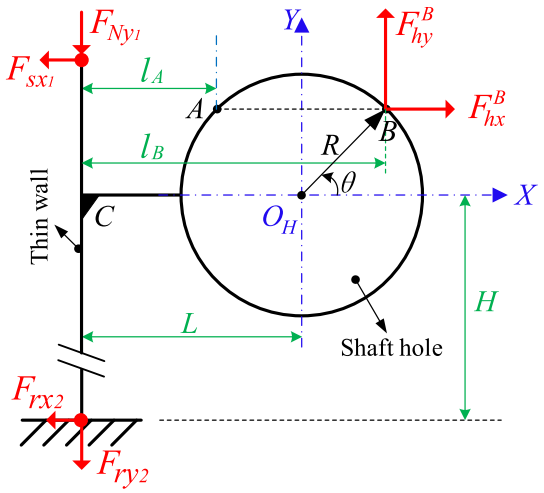

FIGURE 2. Physical model of the cantilever beam of shaft hole on thin wall.

where i =A or B, Δx_{C} and Δy_{C} are the directional offsets at point C of the box thin wall caused by the cutting force.

Due to $\Delta x_{A\phi} \neq \Delta x_{B\phi}$ and $\Delta y_{A\phi} \neq \Delta y_{B\phi}$, there is $k_{hx}^{Ae} \neq k_{hx}^{Be}$ and $k_{hy}^{Ae} \neq k_{hy}^{Be}$. Therefore, through the above derivation, it can be seen that due to the influence of the shaft hole's own structure and the deformation of the thin wall, the directional stiffness of the shaft hole changes with the variation of the machining position. However, this effect has been ignored in the existing boring dynamic models, which will inevitably lead to deviation of the prediction in both the dynamic responses of the boring system and the machined shaft hole surface topography error.

III. BORING DYNAMIC MODELLING OF SHAFT HOLE ON THIN-WALLED BOX

In this section, the analytical expression of the cutting force of the boring system is established, and the calculation model of the directional stiffness of the shaft hole is proposed. On this basis, the boring dynamic model of the shaft hole of the thin-walled box is finally developed.

A. ANALYTICAL EXPRESSION OF CUTTING FORCE

The analysis of cutting forces expressed in different coordinate systems for a single-insert boring is presented in Fig. 3. The rotating coordinate system (r, t, f) is fixed to the boring rod and rotates with the machine tool spindle. The coordinate axis symbols r, t and f successively represent the radial, tangential and feed direction of the boring rod, in which the tangential coordinate axis t is parallel to the cutting speed direction V but opposite. The three-dimensional cutting force in boring is simplified as a concentrated force and acted on the primary cutting edge. The cutting force decomposition reference frame (u, v, w) of the inclined cutting force model is introduced to describe the state of cutting force decomposition. The three-dimensional (3D) Cartesian coordinate system (u, v, w) is defined as: fixed on the front cutting

surface, the origin falls on the primary cutting edge, the v axis is parallel to the cutting speed V direction, the w axis is perpendicular to the plane formed by the straight line between the v axis and the primary cutting edge, and the u axis is perpendicular to the v axis and the w axis respectively. The coordinate axis direction follows the right-hand rule.

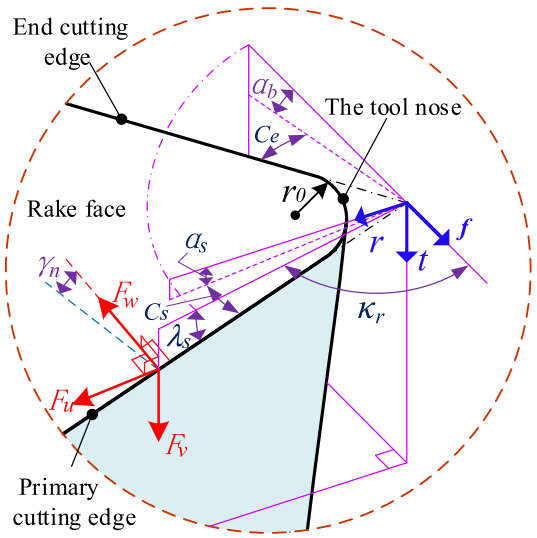

FIGURE 3. The boring single insert geometry and the cutting force analysis.

Sabberwal [9] pointed out that the cutting force is proportional to the cross-sectional area of the chip load. According to the boring experiment in [23], it is found that the cutting force is related to the cutting speed, and there is a certain critical value. Therefore, to improve the prediction accuracy of boring cutting force, a quadratic polynomial cutting force coefficient correction term based on the change of cutting speed is carried out, and the cutting force calculation formula of a single-insert boring cutter can be expressed as [17],

$$\begin{cases} F_u = \left(a_{u0}V^2 + a_{u1}V + a_{u2}\right) \cdot K_{uc} \cdot A_c \\ F_v = \left(a_{v0}V^2 + a_{v1}V + a_{v2}\right) \cdot K_{vc} \cdot A_c \\ F_w = \left(a_{w0}V^2 + a_{w1}V + a_{w2}\right) \cdot K_{wc} \cdot A_c \end{cases} \tag{5}$$

of which, K_{uc}, K_{vc} and K_{wc} represent the cutting force coefficients along u, v and w directions respectively, and their values depend on the boring insert geometry parameters and the material properties of the workpiece and the cutter [24]. A_c refers to the load area of the chip in contact with the rake face without deformation. a_{ik} denotes the quadratic polynomial coefficient of cutting force modified based on the cutting speed, and its subscript symbols $i = u, v, w$ and $k = 0,1, 2$.

The boring insert geometry parameters, such as the cutting edge inclination of the primary cutting edge λ_s, the rake angle of the tool γ_0, the normal rake angle γ_n and the cutting edge angle κ_r can be expressed as,

$$\begin{cases} \lambda_s = \arctan\left[\tan\left(\alpha_s\right) \cdot \cos\left(C_s\right) - \tan\left(\alpha_b\right) \cdot \sin\left(C_s\right)\right] \\ \gamma_0 = \arctan\left[\tan\left(\alpha_s\right) \cdot \sin\left(C_s\right) + \tan\left(\alpha_b\right) \cdot \cos\left(C_s\right)\right] \\ \gamma_n = \arctan\left[\tan\left(\gamma_0\right) \cdot \cos\left(\lambda_s\right)\right] \\ \kappa_r = \arccos\left[\dfrac{\tan\left(\alpha_s\right) \cdot \tan\left(\gamma_0\right) - \tan\left(\alpha_b\right) \cdot \tan\left(\lambda_s\right)}{\tan^2\left(\gamma_0\right) + \tan^2\left(\lambda_s\right)}\right] \end{cases} \tag{6}$$

Since the reference coordinate system (u, v, w) describing the cutting force and the rotating coordinate system (r, t, f) of the boring cutter movement is fixed to the cutter, the transformation relationship of the cutting force in the two coordinate systems can be established, namely,

$$\begin{bmatrix} F_{cr} \\ F_{ct} \\ F_{cf} \end{bmatrix} = \begin{bmatrix} \sin\left(\kappa_r\right) & 0 & \cos\left(\kappa_r\right) \\ 0 & 1 & 0 \\ -\cos\left(\kappa_r\right) & 0 & \sin\left(\kappa_r\right) \end{bmatrix} \cdot \begin{bmatrix} F_u \\ F_v \\ F_w \end{bmatrix} \tag{7}$$

Substitute Eq. (7) into Eq.(1), and the expression of the cutting force in the coordinate system can be obtained,

$$\begin{bmatrix} F_{hx} \\ F_{hy} \\ F_{hz} \end{bmatrix} = \begin{bmatrix} \cos\theta \cdot \sin\left(\kappa_r\right) & \sin\theta & \cos\theta \cdot \cos\left(\kappa_r\right) \\ \sin\theta \cdot \sin\left(\kappa_r\right) & -\cos\theta & \sin\theta \cdot \cos\left(\kappa_r\right) \\ \cos\left(\kappa_r\right) & 0 & -\sin\left(\kappa_r\right) \end{bmatrix} \cdot \begin{bmatrix} F_u \\ F_v \\ F_w \end{bmatrix} \tag{8}$$

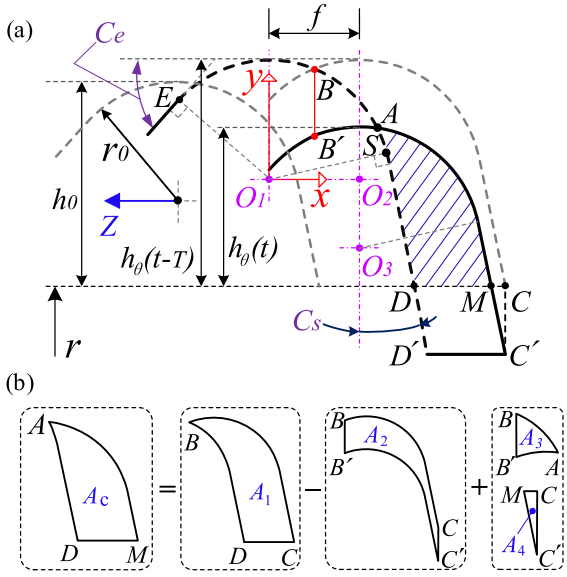

FIGURE 4. Formation analysis of the instantaneous chip load area.

According to Eqs. (5) and (8), the cutting force is related to A_c, namely the area of the undeformed chip in contact with the rake face. Fig. 4 shows the formation analysis of instantaneous chip load area A_c when the single-insert boring is adopted. Boring process is a periodic rotary movement, when the cutting vibration is slight, it can be considered that the instantaneous cutting area of the current cycle is

jointly constrained by the actual cutting contour of the current and previous cutting cycles, which is represented in the blue shadow in Fig. 4.

Since the boring tool tip has a geometric circle shape, the fluctuation of cutting depth h_θ in the adjacent feeding period will cause the nonlinear change of the load area of the instantaneous chip in the current period. To calculate the dynamic change of cutting force accurately, the effect of the cutting rotation period delay should be considered. The instantaneous chip load area A_c can be expressed as,

$$A_c = A_1 - A_2 + A_3 + A_4 \tag{9}$$

In Fig. 4, xO_1y is the established plane local coordinate system. The origin of the coordinate system coincides with the center of the tool tip at time t-T, and the X-axis and Y-axis directions are parallel to the axial and radial directions of the boring bar respectively. Suppose the angle between the line from point O_1 as the starting point to any point on the edge envelope curve $DABE$ at time t-T and the positive direction of the X-axis is φ_1, the sign shows a positive value when angleφ_1 is in the counterclockwise direction. According to the value range of φ_1, the equation $g_1(x_1, y_1)$ of the envelope curve $DABE$ of the cutting edge can be expressed as,

$$g_1(x_1, y_1): \begin{cases} \begin{bmatrix} x_1 \\ y_1 \end{bmatrix} = \dfrac{r_0}{\cos(C_s - \phi_1)} \cdot \begin{bmatrix} \cos\phi_1 \\ \sin\phi_1 \end{bmatrix}, \\ \phi_1 \in (-\pi + C_e, C_s) \\ \begin{bmatrix} x_1 \\ y_1 \end{bmatrix} = r_0 \cdot \begin{bmatrix} \cos\phi_1 \\ \sin\phi_1 \end{bmatrix}, \\ \phi_1 \in [C_s, \pi/2 + C_e] \\ \begin{bmatrix} x_1 \\ y_1 \end{bmatrix} = \dfrac{r_0}{\sin(\phi_1 - C_e)} \cdot \begin{bmatrix} \cos\phi_1 \\ \sin\phi_1 \end{bmatrix}, \\ \phi_1 \in (\pi/2 + C_e, \pi + C_e) \end{cases} \tag{10}$$

According to Eq. (10), the corresponding azimuth angle of points B, E and S in Fig. 4 can be obtained separately: $\varphi_1^{\mathrm{B}} = \arccos(f/2r_0)$, $\varphi_1^{\mathrm{E}} = \pi/2 + C_e$ and $\varphi_1^{\mathrm{S}} = C_s$. The cutting point of the insert at the circular contour of the shaft hole is point D, and the parameter $p_D = h_\theta(t\text{-}T) - r_0(1 - \sin C_s)$ is used to judge whether point D is on the primary cutting edge of the boring tool,

$$\phi_1^D = \begin{cases} \arcsin\left(\dfrac{r_0 - h_\theta(t-T)}{r_0}\right), & p_D \le 0 \\ \arctan\left(\dfrac{[r_0 - h_\theta(t-T)] \cdot \cos C_s}{r_0 - [r_0 - h_\theta(t-T)] \cdot \sin C_s}\right), & p_D > 0 \end{cases} \tag{11}$$

According to the principle of coordinate translation, the coordinate system xO_1y is translated by a feed f in the positive direction of X-axis, and then another local plane coordinate system xO_2y can be established, where the equation $g_2(x_2, y_2)$ of the envelope curve CB of the cutting edge can be written as,

$$g_2(x_2, y_2): \begin{cases} \begin{bmatrix} x_2 \\ y_2 \end{bmatrix} = \dfrac{r_0}{\cos(C_s - \phi_2)} \cdot \begin{bmatrix} \cos\phi_2 \\ \sin\phi_2 \end{bmatrix} + \begin{bmatrix} f \\ 0 \end{bmatrix}, \\ \phi_2 \in (-\pi + C_e, C_s) \\ \begin{bmatrix} x_2 \\ y_2 \end{bmatrix} = r_0 \cdot \begin{bmatrix} \cos\phi_2 \\ \sin\phi_2 \end{bmatrix} + \begin{bmatrix} f \\ 0 \end{bmatrix}, \\ \phi_2 \in [C_s, \pi/2 + C_e] \\ \begin{bmatrix} x_2 \\ y_2 \end{bmatrix} = \dfrac{r_0}{\sin(\phi_2 - C_e)} \cdot \begin{bmatrix} \cos\phi_2 \\ \sin\phi_2 \end{bmatrix} + \begin{bmatrix} f \\ 0 \end{bmatrix}, \\ \phi_2 \in (\pi/2 + C_e, \pi + C_e) \end{cases} \tag{12}$$

The azimuth angle of points B and C in the coordinate system xO_2y can then be deduced as,

$$\begin{cases} \phi_2^B = \pi/2 + \arcsin(f/2r_0) \\ \phi_2^C = \phi_1^D \end{cases} \tag{13}$$

Using the curve equation in Eq. (12), the arc length of BC can be obtained as,

$$g_1(x_1, y_1): \begin{cases} \begin{bmatrix} x_1 \\ y_1 \end{bmatrix} = \dfrac{r_0}{\cos(C_s - \phi_1)} \cdot \begin{bmatrix} \cos\phi_1 \\ \sin\phi_1 \end{bmatrix}, \\ \phi_1 \in (-\pi + C_e, C_s) \\ \begin{bmatrix} x_1 \\ y_1 \end{bmatrix} = r_0 \cdot \begin{bmatrix} \cos\phi_1 \\ \sin\phi_1 \end{bmatrix}, \\ \phi_1 \in [C_s, \pi/2 + C_e] \\ \begin{bmatrix} x_1 \\ y_1 \end{bmatrix} = \dfrac{r_0}{\sin(\phi_1 - C_e)} \cdot \begin{bmatrix} \cos\phi_1 \\ \sin\phi_1 \end{bmatrix}, \\ \phi_1 \in (\pi/2 + C_e, \pi + C_e) \end{cases} \tag{14}$$

Similarly, the coordinate system xO_2y is translated by $\Delta h = h_\theta(t\text{-}T) - h_\theta(t)$ along the y-axis direction to construct the local coordinate system xO_3y, then the equation $g_3(x_3, y_3)$ of the boring tool edge envelope curve C' MAB' in the current cutting cycle can be given as,

$$g_3(x_3, y_3): \begin{cases} \begin{bmatrix} x_3 \\ y_3 \end{bmatrix} = \dfrac{r_0}{\cos(C_s - \phi_3)} \cdot \begin{bmatrix} \cos\phi_3 \\ \sin\phi_3 \end{bmatrix} + \begin{bmatrix} f \\ -\Delta h \end{bmatrix}, \\ \phi_3 \in (-\pi + C_e, C_s) \\ \begin{bmatrix} x_3 \\ y_3 \end{bmatrix} = r_0 \cdot \begin{bmatrix} \cos\phi_3 \\ \sin\phi_3 \end{bmatrix} + \begin{bmatrix} f \\ -\Delta h \end{bmatrix}, \\ \phi_3 \in [C_s, \pi/2 + C_e] \\ \begin{bmatrix} x_3 \\ y_3 \end{bmatrix} = \dfrac{r_0}{\sin(\phi_3 - C_e)} \cdot \begin{bmatrix} \cos\phi_3 \\ \sin\phi_3 \end{bmatrix} + \begin{bmatrix} f \\ -\Delta h \end{bmatrix}, \\ \phi_3 \in (\pi/2 + C_e, \pi + C_e) \end{cases} \tag{15}$$

According to Eq. (15), the corresponding azimuth angles of points B and C in coordinate system xO_3y can be obtained: $\varphi_3^{B\prime} = \varphi_2^B$ and $\varphi_3^{C\prime} = \varphi_2^C$. The azimuth of M is judged

according to $p_M = h_\theta(t)$-r_0(1-sinC_s), that is, $\angle MO_3x$ can be expressed as,

$$g_3(x_3, y_3): \begin{cases} \begin{bmatrix} x_3 \\ y_3 \end{bmatrix} = \dfrac{r_0}{\cos(C_s - \phi_3)} \cdot \begin{bmatrix} \cos\phi_3 \\ \sin\phi_3 \end{bmatrix} + \begin{bmatrix} f \\ -\Delta h \end{bmatrix}, \\ \phi_3 \in (-\pi + C_e, C_s) \\ \begin{bmatrix} x_3 \\ y_3 \end{bmatrix} = r_0 \cdot \begin{bmatrix} \cos\phi_3 \\ \sin\phi_3 \end{bmatrix} + \begin{bmatrix} f \\ -\Delta h \end{bmatrix}, \\ \phi_3 \in [C_s, \pi/2 + C_e] \\ \begin{bmatrix} x_3 \\ y_3 \end{bmatrix} = \dfrac{r_0}{\sin(\phi_3 - C_e)} \cdot \begin{bmatrix} \cos\phi_3 \\ \sin\phi_3 \end{bmatrix} + \begin{bmatrix} f \\ -\Delta h \end{bmatrix}, \\ \phi_3 \in (\pi/2 + C_e, \pi + C_e) \end{cases} \tag{16}$$

Through simultaneous Eqs. (10) and (15), the intersection point A of the envelope curve of the cutting edge at time t-T of the last cycle and the time t of the current cycle can be solved. The azimuth angle $[\varphi_1^A, \varphi_3^A]^T$ corresponding to coordinate system xO_1y and xO_3y can be calculated according to the positive and negative signs of the radial cutting depth fluctuation Δh in the current boring machining cycle:

① When h≥0, that is, the cutting depth $h_\theta(t)$ in the current cutting period is less than $h_\theta(t\text{-}T)$ in the last cutting period. The parameter $p_A = \Delta h$-r_0(1-sinC_s) is constructed to determine whether point A is on the primary cutting edge of the tool tip circle. Then, the piecewise functions applied in Eqs. (10) and (15) can be selected by the positive and negative signs of p_A to solve $[\phi_1^A, \phi_3^A]$,

$$\begin{cases} \begin{bmatrix} \phi_1^A \\ \phi_3^A \end{bmatrix} = \begin{bmatrix} \arctan\frac{f}{\Delta h} - \arcsin\frac{\sqrt{\Delta h^2 + f^2}}{2r_0} \\ \arctan\frac{f}{\Delta h} + \arcsin\frac{\sqrt{\Delta h^2 + f^2}}{2r_0} \end{bmatrix}, \quad p_A \le 0 \\ \begin{bmatrix} \phi_1^A \\ \phi_3^A \end{bmatrix} = \begin{bmatrix} \arctan\frac{r_0\sin\phi_3^A - \Delta h}{r_0\cos\phi_3^A + f} \\ C_s + \arccos\left(\frac{r_0 + \Delta h\sin C_s - f\cos C_s}{r_0}\right) \end{bmatrix}, \quad p_A > 0 \end{cases} \tag{17}$$

② When Δh<0, the discriminant parameters are set as follows,

$$\begin{cases} p_A = \Delta h - r_0\cos C_e + \sqrt{r_0^2 - (f - r_0\sin C_e)^2} \\ p_{As} = -f\tan C_e - r_0\cos C_e + \sqrt{r_0^2 - (f - r_0\sin C_e)^2} \end{cases} \tag{18}$$

Here, P_{As} denotes the discriminant parameter to judge whether the cutting point of the insert is on the tool nose when point A is on the cutting edge of the boring tool pair, and its value is negative.

Similarly, $[\varphi_1^A, \varphi_3^A]$ can be calculated as,

$$\begin{cases} \begin{bmatrix} \phi_1^A \\ \phi_3^A \end{bmatrix} = \begin{bmatrix} \frac{\pi}{2} - \arctan\frac{\Delta h}{f} - \arcsin\frac{\sqrt{\Delta h^2 + f^2}}{2r_0} \\ \frac{\pi}{2} - \arctan\frac{\Delta h}{f} + \arcsin\frac{\sqrt{\Delta h^2 + f^2}}{2r_0} \end{bmatrix}, \quad 0 \le p_A \\ \begin{bmatrix} \phi_1^A \\ \phi_3^A \end{bmatrix} = \begin{bmatrix} \frac{\pi}{2} + C_e - \arccos\left(\frac{r_0 - \Delta h\cos C_e - f\sin C_e}{r_0}\right) \\ \pi + \arctan\left(\frac{r_0\sin\phi_1^A + \Delta h}{r_0\cos\phi_1^A - f}\right) \end{bmatrix}, \quad p_{As} \le p_A < 0 \\ \begin{bmatrix} \phi_1^A \\ \phi_3^A \end{bmatrix} = \begin{bmatrix} C_e + \frac{\pi}{2} \\ \pi + \arctan\left(\tan C_e - \frac{r_0}{(f + r_0\sin C_e)\cos C_e}\right) \end{bmatrix}, \quad p_A < p_{As} \end{cases} \tag{19}$$

Through simultaneous Eqs. (10), (15), (17) and (19), A_1, A_2, A_3 and A_4 can be calculated as follows,

$$A_1 = f \cdot h_\theta(t - T) - \left[f \cdot r_0 - \frac{f}{2}\left(\sqrt{r_0^2 - \left(\frac{f}{2}\right)^2}\right) - r_0^2 \cdot \arcsin\left(\frac{f}{2r_0}\right)\right] \tag{20}$$

$$A_2 = [h_\theta(t - T) - h_\theta(t)] \cdot \left(x_2^C - x_2^B\right) \tag{21}$$

$$A_3 = \int_{\phi_1^B}^{\phi_1^A} y_1 \frac{dx_1}{d\phi} d\phi - \int_{\phi_3^{B'}}^{\phi_3^A} y_3 \frac{dx_3}{d\phi} d\phi \tag{22}$$

$$A_4 = \int_{\phi_3^M}^{\phi_3^{C'}} [h_\theta(t - T) - r_0 - y_3] \frac{dx_3}{d\phi} d\phi \tag{23}$$

Substituting Eqs. (20)-(23) into Eq. (9), the chip area A_c can be obtained, and then the cutting force can also be solved in Eq. (5) accordingly.

From the above derivation, when the fixed boring cutter type and cutting feed f are given, A_c can be expressed as a function of the time variable cutting depth $h_\theta(t)$ and $h_\theta(t\text{-}T)$ of the adjacent cutting periods, namely,

$$A_c(t) = g(h_\theta(t), h_\theta(t - T)) \tag{24}$$

B. MODELLING OF RADIAL STIFFNESS OF SHAFT HOLE ON THE THIN-WALLED BOX

From Fig. 2 we can know that the directional stiffness of the shaft hole changes with the variation of the machining position, which will affect the dynamic characteristics of the boring system. To more accurately express the directional stiffness of the shaft hole, Eq. (4) can be written as,

$$\begin{cases} k_{hx}^{\theta e} = \dfrac{F_{hx}^{\theta}}{\Delta x_{\theta\varphi} + \Delta x_C} \\ k_{hy}^{\theta e} = \dfrac{F_{hy}^{\theta}}{\Delta y_{\theta\varphi} + \Delta y_C} \end{cases} \tag{25}$$

where, $k_{hx}^{\theta e}$ and $k_{hy}^{\theta e}$ denote the equivalent stiffness of the shaft hole along the X and Y axes at position angle θ, respectively.

F_{hx}^{θ} and k_{hy}^{θ} refer to the cutting forces acting on the cutter site at position angle θ. The direction offsets Δx_C and Δy_C at the point C shown in Fig. 2 can be expressed as,

$$\begin{cases} \Delta x_C = F_{hx}^{\theta}/k_{hy}^{C} \\ \Delta y_C = F_{hy}^{\theta}/k_{hy}^{C} \end{cases} \tag{26}$$

Here, k_{hx}^{C} and k_{hy}^{C} represent the directional stiffness at point C, respectively.

Considering that the box wall structure is usually characterized by asymmetry, uneven wall thickness and irregular distribution, a parameter ϕ_{Y0}^{C} that is only related to the structural form of the box wall is proposed and added into the shaft hole radial stiffness model and makes it generally representative. Here, ϕ_{Y0}^{C} represents the unit angle of line segment CO_H caused by the unit force acting on the Y direction of point C in Fig. 2. Replace ϕ_{θ}^{C} in Eq. (4) with $\phi_C = \phi_{\theta}^{C} + F_{hy}^{\theta} \cdot \phi_{Y0}^{C}$, and get,

$$\begin{cases} \Delta x_{\theta\varphi} = \varphi_C \cdot L \cdot \sin(\varphi_C) \\ \Delta y_{\theta\varphi} = \varphi_C \cdot L \cdot \cos(\varphi_C) \end{cases} \tag{27}$$

Combining with Eq. (2), the bending deformation angle ϕ_C=M_{θ}^{C}/I_C can be rewritten as,

$$\varphi_C = \frac{F_{hy}^{\theta} \cdot (L + R\cos\theta)}{I_C} \tag{28}$$

Usually, ϕ_C is a small rotational angle, thus $\sin(\phi_C) \approx \phi_C$ and $\cos(\phi_C) \approx 1$. Eq. (27) can then be simplified as,

$$\begin{cases} \Delta x_{\theta\varphi} = (\varphi_C)^2 \cdot L \\ \Delta y_{\theta\varphi} = \varphi_C \cdot L \end{cases} \tag{29}$$

Since $(\phi_C)^2$ is a higher order minimum, we can consider $\Delta x_{\theta\phi} \approx 0$. Substituting Eqs. (26), (28) and (29) into (25), the calculation formula of the radial equivalent stiffness of the shaft hole on the thin-walled box can be finally obtained as,

$$\begin{cases} k_{hx}^{\theta e} = k_{hx}^{C} \\ k_{hy}^{\theta e} = \dfrac{k_{hy}^{C}}{1 + L \cdot k_{hy}^{C} \cdot \left(\frac{L + R\cos\theta}{I_C}\right)} \end{cases} \tag{30}$$

C. PROPOSED DYNAMIC MODEL OF BORING SYSTEM

Fig. 5 displays the proposed spring-damping system model for boring the shaft hole. In this model, the boring cutter and the shaft hole are assumed to be the concentrated mass objects with two degrees of freedom respectively. Under the excitation of the cutting force fluctuation, the boring cutter and the shaft hole will produce dynamic displacement responses along the X and Y axis respectively, which will cause periodic fluctuation of radial instantaneous cutting depth h_θ(t).

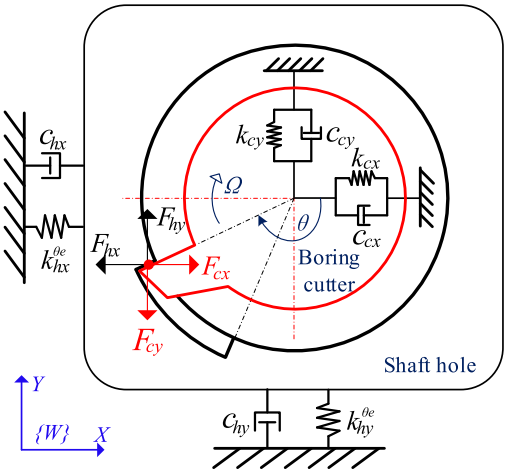

FIGURE 5. The spring-damping system for boring the shaft hole.

According to Newton's law, the differential equation of cutting vibration of the shaft hole and boring cutter can be expressed as follows,

$$\begin{cases} m_h\ddot{x}_h + c_{hx}\dot{x}_h + k_{hx}^{\theta e}x_h = F_{hx} \\ m_h\ddot{y}_h + c_{hy}\dot{y}_h + k_{hy}^{\theta e}y_h = F_{hy} \end{cases} \tag{31}$$

$$\begin{cases} m_c\ddot{x}_c + c_{cx}\dot{x}_c + k_{cx}x_c = F_{cx} \\ m_c\ddot{y}_c + c_{cy}\dot{y}_c + k_{cy}y_c = F_{cy} \end{cases} \tag{32}$$

of which,

$$\begin{cases} \vec{F}_{hx} = -\vec{F}_{cx} \\ \vec{F}_{hy} = -\vec{F}_{cy} \end{cases} \tag{33}$$

In Eqs (31) and (32), m_h and m_c mean equivalent mass of the shaft hole and boring cutter, respectively. c_{hx}, c_{hy}, c_{cx} and c_{cy} represent the equivalent damping of the shaft hole and boring cutter along the X and Y directions separately. $k_{hx}^{\theta e}$, $k_{hy}^{\theta e}$, k_{cx} and k_{cy} denote the equivalent directional stiffness of the shaft hole and boring cutter along the X and Y directions respectively. F_{hx}, F_{hy}, F_{cx} and F_{cy} respectively represent the cutting forces acting on the shaft hole and boring cutter along X and Y directions.

In Fig.1 (b), the displacement vector $\boldsymbol{e}_c$ and $\boldsymbol{e}_h$ of the center of the boring cutter and shaft hole can be calculated as,

$$\begin{cases} |\vec{e}_c| = \sqrt{x_c^2 + y_c^2} \\ |\vec{e}_h| = \sqrt{x_h^2 + y_h^2} \end{cases} \tag{34}$$

The azimuth angles ${}^1\phi_{c\theta}$ and ${}^1\phi_{h\theta}$ of $\boldsymbol{e}_c$ and $\boldsymbol{e}_h$ projected on the XOY plane in coordinate system {W} are expressed as,

$${}^1\varphi_{c\theta} = \arctan\left({}^{y_c}/_{x_c}\right) \tag{35}$$

$${}^1\varphi_{h\theta} = \pi + \arctan\left({}^{y_h}/_{x_h}\right) \tag{36}$$

$$\begin{aligned} h(t) = {} & R - |e_c(t)|\cos\left[\theta(t) - \left(\pi + {}^1\varphi_c(t)\right)\right] - \left|{}^2\vec{e}_h(t)\right|\cos\left[\theta(t) - {}^2\varphi_h(t)\right] \\ & - \sqrt{r^2 - \left[|e_c(t)|\sin\left(\theta(t) - \left(\pi + {}^1\varphi_c(t)\right)\right) + \left|{}^2\vec{e}_h(t)\right|\sin\left(\theta(t) - {}^2\varphi_h(t)\right)\right]^2} \end{aligned} \tag{37}$$

The relation function between the radial cutting depth $h(\theta)$ and $\boldsymbol{e}_c$, $\boldsymbol{e}_h$ has been given in Eq. (9). To facilitate the unified description of variables in the time domain, it can be rewritten as in (37), shown at the bottom of the previous page, of which,

$$\begin{cases} \left|{}^2\vec{e}_h(t)\right| &= \left\{\left|{}^0\vec{e}_h\right|^2 + |e_h(t)|^2 - 2\left|{}^0\vec{e}_h\right| \cdot |e_h(t)| \right. \\ & \left. \cdot \cos\left[\pi - {}^1\varphi_h(t) + {}^1\varphi_0\right]\right\}^{1/2} \\ {}^2\varphi_h(t) &= \arctan\left(\frac{\left|{}^0\vec{e}_h\right| \cdot \sin\left({}^0\varphi_h\right) + y_h(t)}{\left|{}^0\vec{e}_h\right| \cdot \cos\left({}^0\varphi_h\right) + x_h(t)}\right) \end{cases} \tag{38}$$

Substituting Eq. (37) into Eq. (24), the instantaneous cutting force can be obtained by parallel establishing Eqs. (5) and (8). In this study, the dynamic parameters of the boring bar are assumed to be the same, namely, $k_{cx} = k_{cy} = k_{cr} = k_c$ and $c_{cx} = c_{cy} = c_{cr} = c_c$. Finally, the dynamic model of the boring system in the form of the matrix can be described as,

$$\mathbf{M}\ddot{\mathbf{Q}} + \mathbf{C}\dot{\mathbf{Q}} + \mathbf{K}\mathbf{Q} = \mathbf{F} \tag{39}$$

of which

$$M = \begin{bmatrix} m_h \\ m_h \\ m_c \\ m_c \end{bmatrix} \quad C = \begin{bmatrix} c_{hx} \\ c_{hy} \\ c_c \\ c_c \end{bmatrix}$$

$$K = \begin{bmatrix} k^e_{hx}(t) \\ k^e_{hy}(t) \\ k_c \\ k_c \end{bmatrix} \quad Q = \begin{bmatrix} x_h(t) \\ y_h(t) \\ x_c(t) \\ y_c(t) \end{bmatrix}$$

$$F = \begin{bmatrix} F_{hx}(t) \\ F_{hy}(t) \\ F_{cx}(t) \\ F_{cy}(t) \end{bmatrix}$$

IV. VERIFICATION FOR THE PROPOSED DYNAMIC MODEL

To verify the correctness of the proposed boring dynamic model, the FE model of the directional stiffness of the shaft hole on the thin-walled box is firstly conducted. Then the experiment set for validating the dynamic characteristics of the boring system is described.

A. FE VERIFICATION MODEL FOR THE DIRECTIONAL STIFFNESS OF THE SHAFT HOLE

The FE is a universal method to identify the dynamic parameters of complex components [25], [26], [27]. In this section, the radial deformation of the shaft hole under static action is obtained through FE statics analysis, and then the radial stiffness of the shaft hole in different directions can be calculated. The proposed stiffness calculation model, namely Eq. (30), can be verified by comparing with the results obtained from the FE model.

The FE calculation process of the equivalent directional stiffness of the shaft hole on the thin-walled box is displayed in Fig. 6. The specific steps are as follows,

1) Establish the 3D model of the thin-walled box, and define the parameters such as material properties and element type, then generate the FE model of the box. In this simulation, the main parameters are set as: the box material is aluminium alloy 6061-T6, its density ρ =2770 kg/m^3, elastic modulus E = 70 GPa and Poisson's ratio μ =0.33.
2) Fix the bottom plane of the box, and apply the load on the surface of the shaft hole along different directions.
3) Calculate and extract the displacements of the shaft hole center in X and Y directions under the load, and then the directional stiffness of the shaft hole in the two directions can be obtained. Finally, verify the correctness of the proposed model by comparing its calculation results with the results obtained from the FE method.

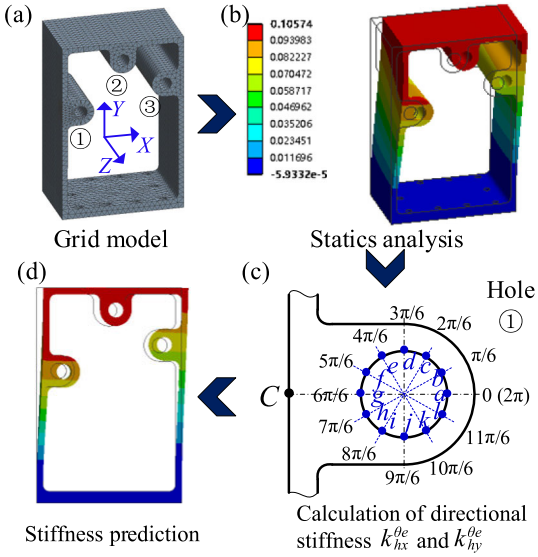

FIGURE 6. FE calculation process of the directional stiffness of the shaft hole.

B. EXPERIMENT SETTING FOR VALIDATING THE PROPOSED BORING DYNAMIC MODEL

The experiment system for verifying the proposed boring dynamic model is shown in Fig. 7, which mainly includes the boring processing system and signal acquisition system.

For the boring processing system, the boring tool used in the experiment is WNC (Winock) four-axis horizontal boring and milling machine. The repeated positioning accuracy of the machine tool is ±0.005 mm, and the effective working space range is 1200 mm×1500 mm×1000 mm. The parameters of the boring tool are presented in Table 1.

For the data acquisition system, the cutting force was acquired using the dynamometer, its type is 9257B, and its measuring range and sensitivity is ±5 KN and 7.5 pC/N, respectively. The spatial coordinates of the characteristic points on the boring machining surface are measured by using FARO manipulator three-coordinate measuring instrument. The sampling frequency of cutting force is 25000 HZ.

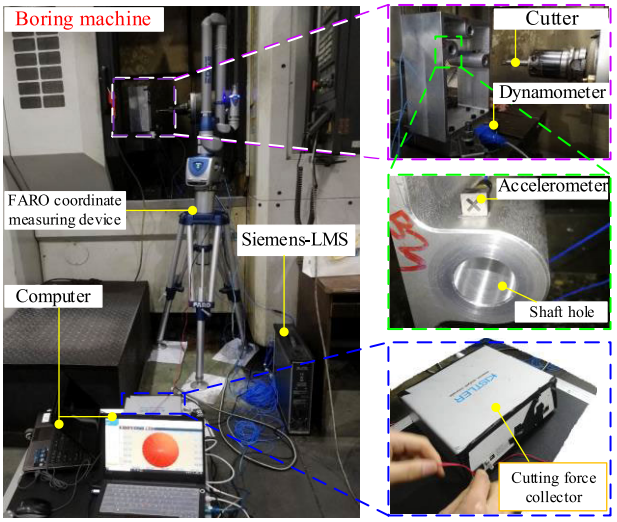

FIGURE 7. The boring dynamic test system.

TABLE 1. Parameters of the boring tool.

Item	Value
Material	45Cr
Type	TPGT110304 PCD
Tool rod length	165 *mm*
Radius of tool rod	11 *mm*
C_s	2°
C_e	32°
r_0	0.2 *mm*
α_s	0°
α_b	0°

V. PROPOSED SURFACE TOPOGRAPHY ERROR PREDICTION METHOD

As described in Section II, the dynamic behavior of the boring system has an important influence on the surface topography of the machined shaft hole. In this section, a cutting scanning surface trajectory model of the single-insert boring cutter is proposed to realize the visualization of the machined surface topography shaft hole. On this basis, a surface topography error prediction method for the boring shaft hole is proposed.

A. MODELLING FOR CUTTING SCANNING SURFACE TRAJECTORY OF THE SINGLE-INSERT BORING CUTTER

To establish the analytical expression of the cutting scanning surface trajectory of the single-insert boring cutter, the layout of each local reference coordinate system of the boring system is established as shown in Fig. 8. Five reference coordinate systems are set in the figure to describe the relative motion relationship between the boring cutter and the shaft hole. In Fig. 8, $\{G\}$ is the global reference coordinate system (machine tool coordinate system), $\{W\}$ refers to the workpiece coordinate system, $\{S\}$ represents the spindle translational coordinate system, $\{C\}$ denotes the local reference coordinate system of the boring insert cutting edge, and $\{F_{pi}\}$ means the local pose coordinate system of any characteristic point p_i on the surface of the shaft hole to be machined. The characteristics and relations of coordinate systems are described as follows,

1) $\{W\}$ belongs to the static coordinate system, also known as the program coordinate system. After the position coordinates $(x_{ow}^G, y_{ow}^G, z_{ow}^G)$ of the origin O_w at $\{G\}$ are determined by the tool setting process, the relative pose relationship between $\{W\}$ and $\{G\}$ is unique.
2) $\{S\}$ is a moving reference system, its origin is fixed on the axis of the nominal boring tool bar and along the axis with the feed speed f relative to the axis hole for translational movement, the coordinate axes O_SX_S, O_SY_S and O_SZ_S are correspondingly parallel or coincide with the O_wX_w, O_wY_w and O_wZ_w coordinate axes of $\{W\}$.

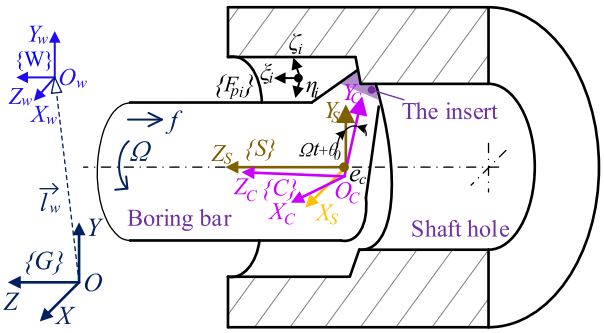

FIGURE 8. The layout of different local reference coordinate systems of the boring system.

3) $\{C\}$ is a moving reference system to describe the cutting edge. Its origin is fixed to the actual knife center point, and the line of coordinate axis O_CY_C and the knife center point and the knife tip center point are merged through the point O_S. The coordinate axis O_CY_C makes a rotary cutting motion with the spindle velocity Ω, and the angle between the coordinate axes O_CY_C and O_SY_S is $\theta = -\Omega t + \theta_0$, where θ_0 is the initial angle of entry.
4) The coordinate axis of $\{F_{pi}\}$ is defined by the unit normal vector η_i of the point p_i on the surface and two mutually perpendicular tangent vectors ξ_i and ξ_i. Due to the circular symmetry of the characteristic surface of the shaft hole, the normal vector η_i generally points to the hole axis, ξ_i is parallel to the cutting velocity direction of the current cutting point, and the tangent vector ξ_i is on the plane formed by η_i and the hole axis.

In the coordinate system $\{W\}$, the regular two-parameter expression of the hole surface can be written as,

$$\mathbf{H} = \mathbf{H}(u, v), \ (u, v) \in D \subset \Re^2 \tag{40}$$

For the nominal feature point p_i on the hole-forming surface, its two-parameter motion coordinate system can be described as,

$$\mathbf{H}_i(u,v):\{\zeta_i(u,v),\xi_i(u,v),\eta_i(u,v)\} \tag{41}$$

To establish the relation between coordinate system $\{W\}$ and $\{F_{pi}\}$, an orthogonal coordinate network is established on the hole-forming surface. $\mathbf{H}(u,v)$ is carried out to represent the radial diameter on the surface, and the orthogonal unit vectors η_i, ξ_i and ζ_i are selected as the coordinate axis directions of $\{F_{pi}\}$, namely,

$$\begin{cases} \zeta_i\left(r_{it1}^{11},r_{it1}^{12},r_{it1}^{13}\right)=\left(\dfrac{\partial\mathbf{H}/\partial u}{\left\|\partial\mathbf{H}/\partial u\right\|}\right)^T \\ \xi_i\left(r_{it2}^{21},r_{it2}^{22},r_{it2}^{23}\right)=\left(\dfrac{\partial\mathbf{H}/\partial v}{\left\|\partial\mathbf{H}/\partial v\right\|}\right)^T \\ \eta_i\left(r_{in}^{31},r_{in}^{32},r_{in}^{33}\right)=\zeta_i\times\xi_i \\ =\left(\dfrac{\left(\partial\mathbf{H}/\partial u\right)\times\left(\partial\mathbf{H}/\partial v\right)}{\left\|\left(\partial\mathbf{H}/\partial u\right)\times\left(\partial\mathbf{H}/\partial v\right)\right\|}\right)^T \end{cases} \tag{42}$$

In Eq. (42), η_i, ξ_i and ζ_i all belong to the 3D vector $\Re^3$.

The parameters α_i, β_i and γ_i are constructed to represent the rotation angles of $\{F_{pi}\}$ around the X, Y and Z axes of $\{W\}$, respectively. Then the rotation transformation matrix of coordinate system $\{F_{pi}\}$ relative to $\{W\}$ can be obtained,

$$\begin{aligned} &{}^{\{W\}}_{\{F_{pi}\}}R_e(\alpha_i,\beta_i,\gamma_i) \\ &=\begin{bmatrix} c\beta_i c\gamma_i & s\alpha_i s\beta_i c\gamma_i-c\alpha_i s\gamma_i & c\alpha_i s\beta_i c\gamma_i+s\alpha_i s\gamma_i \\ c\beta_i s\gamma_i & s\alpha_i s\beta_i s\gamma_i+c\alpha_i c\gamma_i & c\alpha_i s\beta_i s\gamma_i-s\alpha_i c\gamma_i \\ -s\beta_i & s\alpha_i c\beta_i & c\alpha_i c\beta_i \end{bmatrix} \end{aligned} \tag{43}$$

where $s\alpha_i=\sin\alpha_i$, $c\alpha_i=\cos\alpha_i$, and other parameters are analogous.

From the given rotation matrix (43), find the equivalent rotation angles α_i, β_i and γ_i around x-y-z, let,

$${}^{\{W\}}_{\{F_{pi}\}}\boldsymbol{R}_e(\alpha_i,\beta_i,\gamma_i)=\begin{bmatrix}\zeta_i\\ \xi_i\\ \eta_i\end{bmatrix}^T=\begin{bmatrix} r_{it1}^{11} & r_{it2}^{21} & r_{in}^{31} \\ r_{it1}^{12} & r_{it2}^{22} & r_{in}^{32} \\ r_{it1}^{13} & r_{it2}^{23} & r_{in}^{33}\end{bmatrix} \tag{44}$$

Combining Eqs. (43) and (44), it can be concluded that,

$$\cos\beta_i=\sqrt{\left(r_{it1}^{11}\right)^2+\left(r_{it1}^{12}\right)^2} \tag{45}$$

Introduce the bivariate inverse tangent function Atan2(y,x). According to the value of β_i, the values of α_i, β_i and γ_i can be described as following three cases,

1) When $\cos\beta_i\neq 0$

$$\begin{cases} \alpha_i=\mathrm{Atan2}\left(r_{it2}^{23},r_{in}^{33}\right) \\ \beta_i=\mathrm{Atan2}\left(-r_{it1}^{13},\sqrt{\left(r_{it1}^{11}\right)^2+\left(r_{it1}^{12}\right)^2}\right) \\ \gamma_i=\mathrm{Atan2}\left(r_{it1}^{12},r_{it1}^{11}\right) \end{cases} \tag{46}$$

2) When $\beta_i=\pi/2$

$$\begin{cases} \alpha_i=\mathrm{Atan2}\left(r_{it2}^{21},r_{it2}^{22}\right) \\ \beta_i=\pi/2 \\ \gamma_i=0 \end{cases} \tag{47}$$

3) When $\beta_i=$ -$\pi/2$

$$\begin{cases} \alpha_i=-\mathrm{Atan2}\left(r_{it2}^{21},r_{it2}^{22}\right) \\ \beta_i=-\pi/2 \\ \gamma_i=0 \end{cases} \tag{48}$$

The homogeneous transformation matrix of $\{W\}$ relative to $\{F_{pi}\}$ is,

$$\begin{aligned} &{}^{\{W\}}_{\{F_{pi}\}}T \\ &=\begin{bmatrix} \left({}^{\{W\}}_{\{F_{pi}\}}R_e(\alpha_i,\beta_i,\gamma_i)\right)^T & -\left({}^{\{W\}}_{\{F_{pi}\}}R_e(\alpha_i,\beta_i,\gamma_i)\right)^T\cdot{}^W r_{pi} \\ 0\,1 \end{bmatrix} \end{aligned} \tag{49}$$

where, ${}^W\mathbf{r}_{pi}=(x_{opi}^W,y_{opi}^W,z_{opi}^W)^T$ is the position vector of the origin of $\{F_{pi}\}$ in $\{W\}$.

Taking into account the deformation of the box wall in the boring process, it can be,

$$\begin{cases} x_{opi}^W=x_{os}^W+R\cos u+f_x t+x_{h0}+x_h \\ y_{opi}^W=y_{os}^W+R\sin u+f_y t+y_{h0}+y_h \\ z_{opi}^W=z_{os}^W+f_z t+z_{h0}+z_h \end{cases} \tag{50}$$

Here, $\boldsymbol{f}=(f_x,f_y,f_z)^T$ is the feed velocity vector of the cutter center point, and $\boldsymbol{O}_s^w=(x_{os}^w,y_{os}^w,z_{os}^w)^T$ refers to the initial position vector of the origin O_S of $\{S\}$ in $\{W\}$. ${}^0\mathbf{e}_h=(x_{h0},y_{h0},z_{h0})^T$ denotes the coordinate of the deviation vector of the shaft hole position in the initial clamping state. $\mathbf{e}_h=(x_h,y_h,z_h)^T$ represents the instantaneous eccentric vector coordinate of the origin of $\{F_{pi}\}$ deviating from its nominal position, which is related to the vibration of the box wall.

To obtain the relationship between the cutting point of the boring cutter and the nominal feature point to be processed on the hole-forming surface, the position relationship of the cutting point in the coordinate system $\{C\}$ of the boring insert, that is, the position relationship of any cutting point E_i in $\{C\}$ is established and shown in Fig. 9. In Fig. 9, O_r is the center of the tool nose circle of the boring insert and its radius is r_0. κ_r denotes the cutting edge angle of the boring insert, κ_r' means the trail edge angle, R represents the nominal radius of the finished hole and h_0 refers to the nominal depth of cut.

The position coordinates of point E_i in coordinate system $\{C\}$ are described as,

$$\begin{pmatrix} x_{Ei}^C \\ y_{Ei}^C \\ z_{Ei}^C \end{pmatrix}=\begin{pmatrix} 0 \\ (R-r_0)+|O_rE_i|\cdot\sin\phi_i \\ -|O_rE_i|\cdot\cos\phi_i \end{pmatrix} \tag{51}$$

where φ_i represents the angle between unit vector -$\boldsymbol{Z}_c$ and vector $\boldsymbol{O}_r\boldsymbol{E}_r$.

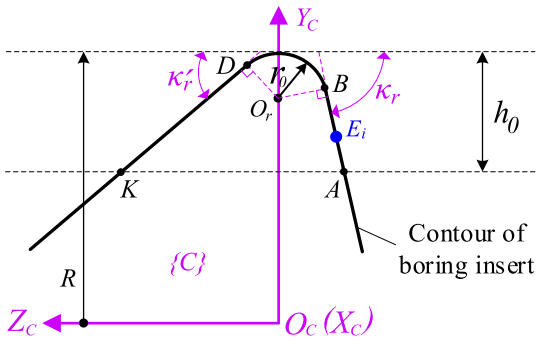

FIGURE 9. Position of the cutting point E_i in the coordinate system {C}.

Combining with Eq. (10), the length value $|O_rE_r|$ can be expressed as,

$$|O_rE_i| = \begin{cases} \dfrac{r_0}{\sin(\kappa_r+\phi_i)}, & \phi_i \in (-\pi+\kappa_r', \pi/2-\kappa_r) \\ r_0, & \phi_i \in [\pi/2-\kappa_r, \pi/2+\kappa_r'] \\ \dfrac{r_0}{\sin(\phi_i-\kappa_r')}, & \phi_i \in (\pi/2+\kappa_r', \pi+\kappa_r') \end{cases} \tag{52}$$

The homogeneous coordinate transformation matrix of $\{C\}$ relative to $\{W\}$ is,

$${}^{W}_{C}T = \begin{bmatrix} \cos\theta & -\sin\theta & 0 & x_{os}^{W}+f_xt+x_c \\ \sin\theta & \cos\theta & 0 & y_{os}^{W}+f_yt+y_c \\ 0 & 0 & 1 & z_{os}^{W}+f_zt+z_c \\ 0 & 0 & 0 & 1 \end{bmatrix} \tag{53}$$

of which, $\mathbf{e}_c = (x_c, y_c, z_c)^T$ is the instantaneous eccentric vector coordinate of the origin O_c of $\{C\}$ in $\{S\}$, which is related to the vibration of the boring bar and can be obtained according to the vibration displacement calculated by the dynamic model of the boring system proposed in Section III.

After combining Eqs. (42)-(50) and (53), the universal coordinate transformation matrix of $\{C\}$ with respect to $\{F_{pi}\}$can be obtained, namely, as in (54), shown at the bottom of the page.

Usually, the axis of the lathe spindle is parallel to the directrix of the shaft hole cylinder when fine boring. Therefore, the pose unit vector of the directrix of the shaft hole cylinder with respect to {W} is assumed to be $(0, 0, 1)^{\mathrm{T}}$. Then Eq. (40) can be further described as,

$$\begin{aligned} \mathbf{H}(u, v) &= (R\cos u, R\sin u, v) \\ &= (R\cos u, R\sin u, 0) \\ &\quad + v(0, 0, 1), (u, v) \in D \subset \Re^2 \end{aligned} \tag{55}$$

Taking the external normal direction of the shaft hole surface as positive, and substituting Eq. (55) into Eq. (42), then combining with Eq. (44), we can get,

$$\begin{bmatrix} \zeta_i \\ \xi_i \\ \eta_i \end{bmatrix}^T = \begin{bmatrix} r_{it1}^{11} & r_{it2}^{21} & r_{in}^{31} \\ r_{it1}^{12} & r_{it2}^{22} & r_{in}^{32} \\ r_{it1}^{13} & r_{it2}^{23} & r_{in}^{33} \end{bmatrix} = \begin{bmatrix} \sin u & 0 & -\cos u \\ -\cos u & 0 & -\sin u \\ 0 & 1 & 0 \end{bmatrix} \tag{56}$$

In the actual boring process, the edge point E_i and the hole surface characteristic point p_i should have the same position azimuth angle in the corresponding time domain, and the hole radius value R is much larger than $\boldsymbol{e}_h$ and $\boldsymbol{e}_c$, then we can set $u = \pi/2+\theta$. Considering that the axial stiffness of the cutter rod and shaft hole is relatively large, all small quantities in the Z direction can be omitted, then Eq. (54) can be further simplified as,

$${}^{p_i}_{E_i}T = \begin{bmatrix} 1 & 0 & 0 & [x_c-(x_h+x_{h0})]\cos\theta+[y_c-(y_h+y_{h0})]\sin\theta \\ 0 & 0 & 1 & 0 \\ 0 & -1 & 0 & R+[x_c-(x_h+x_{h0})]\sin\theta-[y_c-(y_h+y_{h0})]\cos\theta \\ 0 & 0 & 0 & 1 \end{bmatrix} \tag{57}$$

To obtain the position vector $(x_{Ei}^{pi}, y_{Ei}^{pi}, z_{Ei}^{pi})$ of any cutting edge point E_i of the boring cutter in $\{F_{pi}^{f}\}$, through premultiply Eq. (57) by (51), the cutting scanning surface trajectory of the boring cutter can be finally expressed as,

$$\begin{cases} x_{E_i}^{pi} = [x_c-(x_h+x_{h0})]\cos\theta+[y_c-(y_h+y_{h0})]\sin\theta \\ y_{E_i}^{pi} = -|O_rE_i|\cdot\cos\phi_i \\ z_{E_i}^{pi} = r_0-|O_rE_i|\cdot\sin\phi_i+[x_c-(x_h+x_{h0})]\cos\theta \\ \quad +[y_c-(y_h+y_{h0})]\sin\theta \end{cases} \tag{58}$$

B. PROPOSED SURFACE TOPOGRAPHY PREDICTION METHOD FOR BORING SHAFT HOLE

Due to the vibration of the cutter and shaft hole in the boring operation, the end cutting edge near the tool nose may be cut to the machined contour of the last cycle and then form a new shape contour. Therefore, it is necessary to take the minimum cutting residual height scanned by the insert as the contour of the final forming surface. Based on Eq. (58), the problem of solving the local residual height of the boring cutting-formed surface can be transformed into a nonlinear programming optimization problem, namely,

$$\begin{cases} \textit{Minimize} \\ \left\{\Delta_p = z_p\left(\Omega, f, h_0, \phi_i, r_0, \kappa_r, \kappa_r', R, e_c, e_h, {}^{0}e_h, t\right)\right\} \\ \text{Subject to } \phi_i \in [\phi_A, \phi_K] \end{cases} \tag{59}$$

$$\begin{aligned} {}^{F_{pi}}_{C}T &= {}^{F_{pi}}_{W}T \cdot {}^{W}_{C}T \\ &= \begin{bmatrix} r_{it1}^{11}\cos\theta+r_{it1}^{12}\sin\theta & -r_{it1}^{11}\cos\theta+r_{it1}^{12}\sin\theta & r_{it1}^{13} & \zeta_i\left(O_S^W+ft+e_c-{}^{W}r_{pi}\right) \\ r_{it2}^{21}\cos\theta+r_{it2}^{22}\sin\theta & -r_{it2}^{21}\cos\theta+r_{it2}^{22}\sin\theta & r_{it2}^{23} & \xi_i\left(O_S^W+ft+e_c-{}^{W}r_{pi}\right) \\ r_{in}^{31}\cos\theta+r_{in}^{32}\sin\theta & -r_{in}^{31}\cos\theta+r_{in}^{32}\sin\theta & r_{in}^{33} & \eta_i\left(O_S^W+ft+e_c-{}^{W}r_{pi}\right) \\ 0 & 0 & 0 & 1 \end{bmatrix} \end{aligned} \tag{54}$$

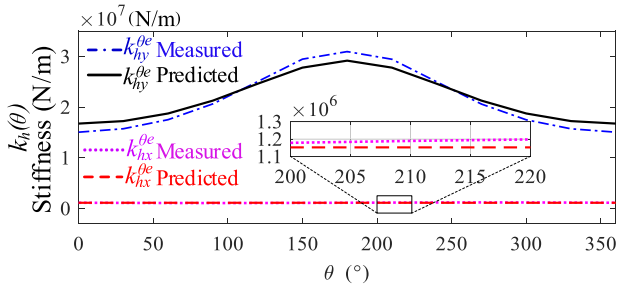

FIGURE 10. Validation results of the radial stiffness of shaft hole.

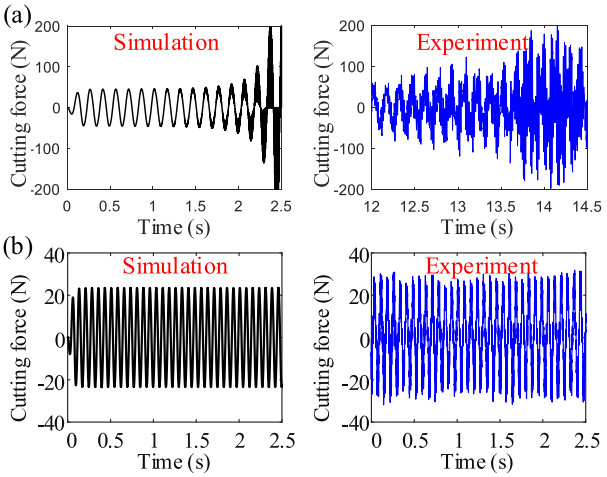

FIGURE 11. Comparison between simulated and measured values of the force: (a) Case #1, (b) Case #2.

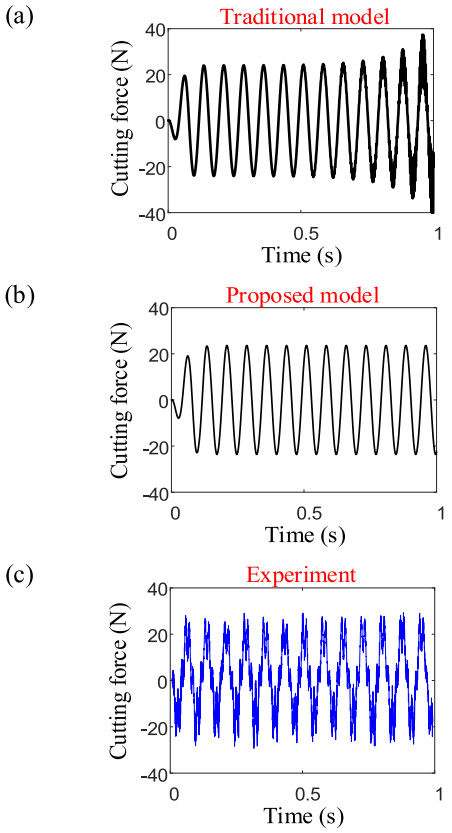

FIGURE 12. Comparison results obtained from different dynamic models and the experiment.

where, φ_i is the azimuth angle in $\{C\}$ of any cutting edge point that may participate in cutting, which is a range value. The initial deviation of box hole position ${}^0\mathbf{e}$ is a constant when the box workpiece is clamped. The instantaneous position offsets $\mathbf{e}_h$ and $\mathbf{e}_c$ of the shaft hole center and the cutter center can be obtained by the proposed boring dynamic model. By solving the nonlinear programming problem of Eq. (59), the residual height of each nominal feature point along the normal direction can be obtained, and then the envelope surface is constructed based on the residual height of each point to form the surface topography of the machining shaft hole.

VI. RESULTS AND DISCUSSION

A. VERIFICATION RESULT ANALYSIS OF THE PROPOSED HOLE DIRECTIONAL STIFFNESS MODEL

The comparison between the analytical stiffness model and the FE model is displayed in Fig. 10. As can be seen that the curve variation of the predicted stiffness value obtained from the proposed model converges with the FE simulation value. It can be calculated that the prediction deviation rates of $k_{hx}^{\theta e}$ and $k_{hy}^{\theta e}$ within the period $(0, 2\pi)$ are within 7% and 11%, respectively. The comparison results verify the correctness of the proposed calculation model of the radial stiffness of the shaft hole.

B. ANALYSIS OF VALIDATION RESULTS OF THE PROPOSED DYNAMIC MODEL

Table 2 shows the equivalent dynamic parameters of the boring system used in the simulation and test. Based on the data in Table 2, the proposed boring dynamic model is solved to obtain the dynamic cutting force and displacement response. Then the results are compared with the experimental results to verify the effectiveness of the proposed dynamic model.

TABLE 2. Dynamic parameters of the hole boring used in simulation and test.

Parameters	Boring cutter	Shaft hole
Equivalent mass (kg)	m_c=4.5	m_h=10.7
Equivalent damping (N·s/m)	c_{cx} = 102.7	c_{hx} = 81.3
	c_{cy} = 101.4	c_{hy} = 110.6
Equivalent stiffness (N/m)	k_{cx} =1.439E6	k_{hx} =1.139E6
	k_{cy} =1.365E6	k_{hy}=(2.33-0.61cosθ)E7

Stable cutting condition is the desired boring state. However, when the selected combination of cutting feed and cutting speed parameters is distributed in the unstable cutting

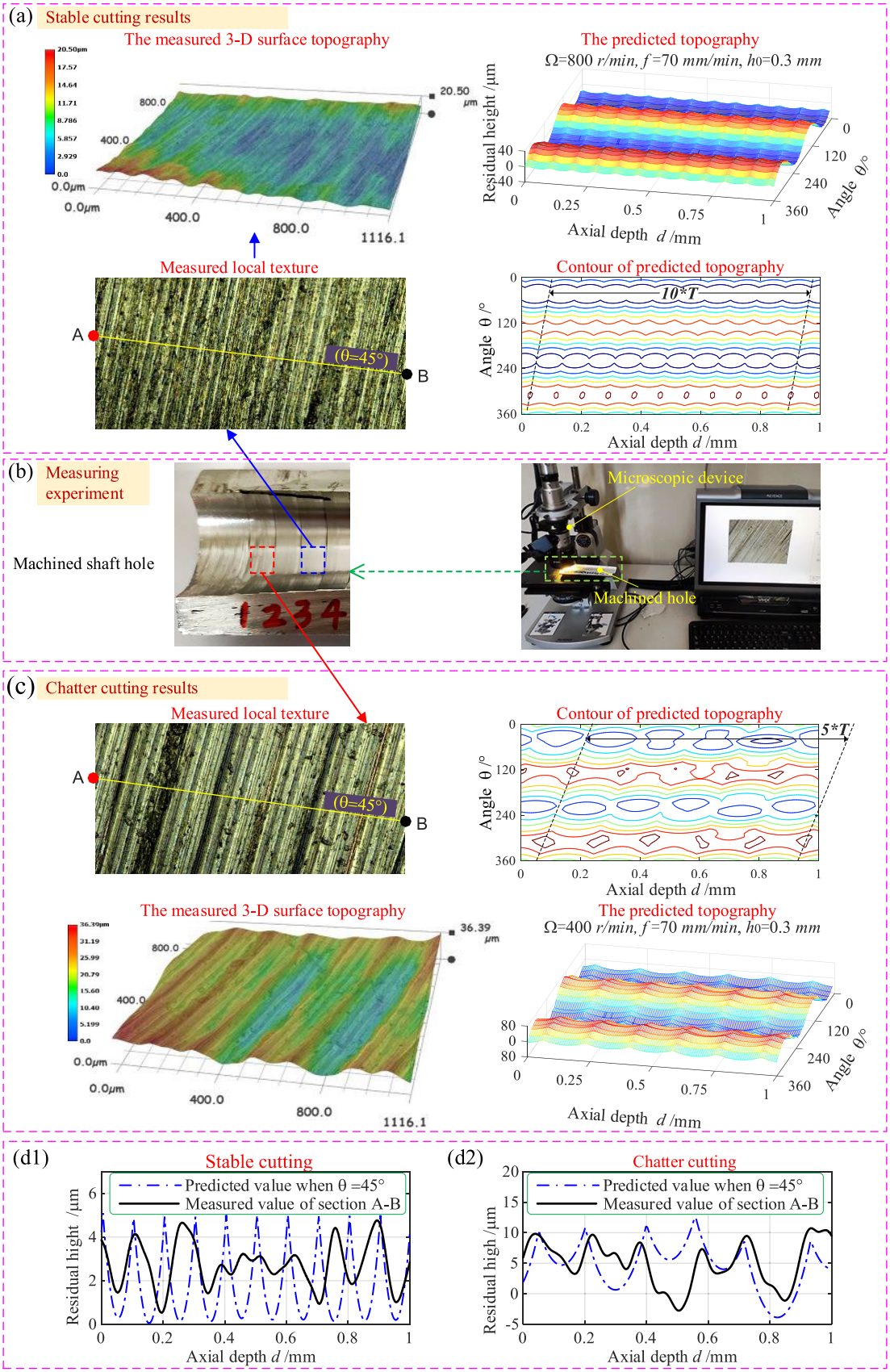

FIGURE 13. Comparison of measured and predicted results of the surface topography of shaft hole.

region of the Lobe diagram of the boring shaft hole, the chatter will occur and further affect the machining quality of the hole surface. Therefore, to verify the proposed dynamic model universality, both cutting states are considered in this comparison study, which are shown in Case #1 (chatter) and Case #2 (stable) in Table 3.

TABLE 3. Boring parameters of the stable and chatter cutting cases.

Parameters	Case #1	Case #2
Cutting feed f (mm/min)	70	70
Cutting depth h_0 (mm)	0.3	0.3
Cutting speed (Rev/min)	400	800
Hole-formed radius (mm)	13.5	13.5

The comparison results of cutting forces in the stable and chatter cutting cases obtained by the proposed model and the test are shown in Fig. 11. It can be seen that the changing trend of the cutting force calculated by the proposed dynamic model fits well with that of the measured value in both the stable and chatter cutting cases, which indicates the effectiveness and universality of the proposed boring dynamic model.

To validate the influence of the radial stiffness of the shaft hole on the boring cutting characteristics, the cutting force obtained from the traditional model in [18] without considering the stiffness, the dynamic model proposed in this paper and experiment are compared and presented in Fig. 12. The prediction results of the traditional model show that the cutting force will appear chatter phenomenon, while the proposed model and test results present that the cutting force are both in a stable cutting state. Due to that considering the flexible support of the shaft hole will produce a vibration absorption effect when boring, thus the results obtained from the proposed model are more consistent with the actual situation.

C. ANALYSIS OF MACHINING TOPOGRAPHY ERROR PREDICTION RESULTS

On the basis of verifying the proposed dynamic model, the surface topography of the shaft hole to be machined is predicted based on the proposed topography prediction method, and then the predicted results are compared with the measured results to verify the correctness of the proposed models and method.

The comparison between the measured results and the predicted results based on the proposed method is displayed in Fig. 13. In the surface measurement experiment, the VHX-7000 ultra depth of field 3D micro-graph (see Fig. 13(b)) is used to measure the surface topography of the shaft hole, which can observe and obtain the point cloud data of the measured surface, and then the topography reconstruction of the measured surface can be realized by using 3D software.

It can be seen in Fig. 13 (a), the 3D topography and contour of the hole surface predicted based on the proposed model have high similarity with the measured results. From the comparison of contour residual height results in the stable cutting case (pictured in Fig. 13 (d1)), it can be seen that the residual peak-valley difference values of the hole profile at the same azimuth angle θ =45 are roughly similar. The predicted maximum peak-valley difference is 5.088 μm while the measured one is 4.232 μm, and it can be calculated that the measured peak-valley value is 16.82% smaller than the predicted one.

Fig. 13 (c) and (d2) show the comparison results between the measured and predicted topography and the residual peak heights. It can be observed that the predicted and measured hole surface topography both agree well and the topography amplitude of the peak-valley difference of the residual profile under this condition both increase exponentially compared with that under the stable cutting condition. The predicted maximum peak-valley difference is 16.351 μm and the measured one is 13.501 μm, their difference reaches 17.27%.

On the whole, the measured and predicted residual heights of the hole profile fluctuate around the mean residual heights under both the stable and chatter cutting conditions, which indicates the correctness of the proposed surface topography error prediction method for the boring shaft hole.

VII. CONCLUSION

The traditional boring dynamic model ignores the influence of the radial deformation of the shaft hole of the thin-walled box on the boring dynamic characteristics, which will lead to a deviation in the prediction of the machining topography error of the shaft hole. To solve this problem, a new radial stiffness calculation model of the shaft hole on the thin-walled box is established and verified by the FE method. Moreover, a dynamic model of the boring system is developed, and the experimental verification of the presented dynamic model is also carried out. Combining with the proposed dynamic model, a prediction method of machining topography error of the shaft hole is proposed, and the prediction and measurement analysis of the shaft hole topography error are finally carried out. Through this research, some main conclusions can be drawn as follows:

- The proposed radial stiffness calculation model of the shaft hole on the thin-walled box can achieve high calculation accuracy, the FE verification shows that the calculation errors of the hole radial stiffness in the X and Y directions of the proposed model are within 7% and 11%, respectively.
- The experimental results of boring dynamic characteristics show that the proposed boring dynamic model can accurately predict the real cutting force fluctuation state of the boring system, and the influence of the radial stiffness of the shaft hole on the boring dynamic behavior can not be ignored.
- The proposed surface topography error prediction method shows good performance by comparing with the measured surface topography error.

ACKNOWLEDGMENT

The authors are grateful to the National Natural Science Foundation of China (Grant No. 52035002 and 51475053).

DECLARATION OF COMPETING INTEREST

The authors declare that they have no competing financial interests or personal relationships that could have appeared to influence the work reported in this paper.

REFERENCES

[1] X. Yang, L. Zhang, W. Xie, and J. Zhang, "Sequential and iterative distributed model predictive control of multi-motor driving cutterhead system for TBM," *IEEE Access*, vol. 7, pp. 46977–46989, 2019.

[2] L. Yang, L. Wang, W. Yu, and Y. Shao, "Investigation of tooth crack opening state on time varying meshing stiffness and dynamic response of spur gear pair," *Eng. Failure Anal.*, vol. 121, Mar. 2021, Art. no. 105181.

[3] Q. Zeng, G. Feng, Y. Shao, F. Gu, and A. D. Ball, "Planetary gear fault diagnosis based on an instantaneous angular speed measurement system with a dual detector setup," *IEEE Access*, vol. 8, pp. 66228–66242, 2020.

[4] L. Wang, G. Gong, H. Yang, X. Yang, and D. Hou, "The development of a high-speed segment erecting system for shield tunneling machine," *IEEE/ASME Trans. Mechatronics*, vol. 18, no. 6, pp. 1713–1723, Dec. 2013.

[5] J. Huo, N. Hou, W. Sun, L. Wang, and J. Dong, "Analyses of dynamic characteristics and structure optimization of tunnel boring machine cutter system with multi-joint surface," *Nonlinear Dyn.*, vol. 87, no. 1, pp. 237–254, Jan. 2017.

[6] X. Liang, M. J. Zuo, and Z. Feng, "Dynamic modeling of gearbox faults: A review," *Mech. Syst. Signal Process.*, vol. 98, pp. 852–876, Jan. 2018.

[7] J. Grum and M. Kisin, "The influence of the microstructure of three Al–Si alloys on the cutting-force amplitude during fine turning," *Int. J. Mach. Tools Manuf.*, vol. 46, nos. 7–8, pp. 769–781, Jun. 2006.

[8] E. Budak and E. Ozlu, "Analytial modeling of chatter stability in turning and boring operations: A multi-dimensional approach," *CIRP Ann.*, vol. 56, pp. 401–404, Jan. 2007.

[9] A. Sabberwal, "Chip section and cutting force during the milling operation," *CIRP Ann. Manuf. Techn.*, vol. 10, no. 3, pp. 197–203, 1961.

[10] G. Subramani, R. Suvada, S. Kapoor, R. DeVor, and W. Meingast, "A model for the prediction of force system for cylinder boring process," in *Proc. XV NAMRC*, 1987, pp. 439–446.

[11] F. Kuster and P. E. Gygax, "Cutting dynamics and stability of boring bars," *CIRP Ann.*, vol. 39, no. 1, pp. 361–366, 1990.

[12] F. Atabey, I. Lazoglu, and Y. Altintas, "Mechanics of boring processes Part—I" *Int. J. Mach. Tool. Manu.*, vol. 43, pp. 463–476, Apr. 2003.

[13] H. T. Young, P. Mathew, and P. L. B. Oxley, "Allowing for nose radius effects in predicting the chip flow direction and cutting forces in bar turning," *Proc. Inst. Mech. Eng., C, J. Mech. Eng. Sci.*, vol. 201, no. 3, pp. 213–226, May 1987.

[14] J. Wang and P. Mathew, "Development of a general tool model for turning operations based on a variable flow stress theory," *Int. J. Mach. Tools Manuf.*, vol. 35, no. 1, pp. 71–90, Jan. 1995.

[15] D. Bilgili, E. Budak, and Y. Altintas, "Multibody dynamic modeling of five-axis machine tools with improved efficiency," *Mech. Syst. Signal Process.*, vol. 171, May 2022, Art. no. 108945.

[16] I. Lazoglu, F. Atabey, and Y. Altintas, "Dynamics of boring processes: Part III-time domain modeling," *Int. J. Mach. Tools Manuf.*, vol. 42, no. 14, pp. 1567–1576, Nov. 2002.

[17] E. Ozlu and E. Budak, "Analytical modeling of chatter stability in turning and boring operations—Part I: Model development," *J. Manuf. Sci. Eng.*, vol. 129, no. 4, pp. 726–732, Aug. 2007.

[18] B. Moetakef-Imani and N. Z. Yussefian, "Dynamic simulation of boring process," *Int. J. Mach. Tools Manuf.*, vol. 49, no. 14, pp. 1096–1103, Nov. 2009.

[19] M. H. Miguélez, L. Rubio, J. A. Loya, and J. Fernández-Sáez, "Improvement of chatter stability in boring operations with passive vibration absorbers," *Int. J. Mech. Sci.*, vol. 52, no. 10, pp. 1376–1384, Oct. 2010.

[20] S. Ghorbani, V. A. Rogov, A. Carluccio, and P. S. Belov, "The effect of composite boring bars on vibration in machining process," *Int. J. Adv. Manuf. Technol.*, vol. 105, nos. 1–4, pp. 1157–1174, Nov. 2019.

[21] S. Chockalingam, S. Ramabalan, and K. Govindan, "Chatter control and stability analysis in cantilever boring bar using FEA methods," *Mater. Today, Proc.*, vol. 33, pp. 2577–2580, Jan. 2020.

[22] M. Fallah and B. Moetakef-Imani, "Investigation on nonlinear dynamics and active control of boring bar chatter," *J. Brazilian Soc. Mech. Sci. Eng.*, vol. 43, no. 3, pp. 1–27, Mar. 2021.

[23] N. Z. Yussefian, B. Moetakef-Imani, and H. El-Mounayri, "The prediction of cutting force for boring process," *Int. J. Mach. Tools Manuf.*, vol. 48, nos. 12–13, pp. 1387–1394, Oct. 2008.

[24] K. Mao, M. Zhu, W. Xiao, and B. Li, "A method of using turning process excitation to determine dynamic cutting coefficients," *Int. J. Mach. Tools Manuf.*, vol. 87, pp. 49–60, Dec. 2014.

[25] D. Peng, L. Wang, C. K. Mechefske, and Y. Shao, "Position prediction and error compensation for a large thin-walled box-shaped workpiece in a fixture," *Int. J. Adv. Manuf. Technol.*, vol. 116, nos. 7–8, pp. 2633–2649, Jul. 2021.

[26] R.-C. Dong, Q.-J. Guo, W. Yuan, W. Du, X.-H. Yang, and Y.-J. Zhao, "The finite element model of seated whole human body for vibration investigations of lumbar spine in complex system," *IEEE Access*, vol. 8, pp. 125046–125055, 2020.

[27] L. Yang, L. Wang, Y. Shao, C. K. Mechefske, and Q. Chen, "A new calculation method for tooth fillet foundation stiffness of cracked spur gears," *Eng. Failure Anal.*, vol. 121, Mar. 2021, Art. no. 105173.

DINGQIANG PENG received the B.S. degree in mechanical engineering from the University of Science and Technology, Beijing, China, in 2009. He is currently pursuing the Ph.D. degree in mechanical engineering with Chongqing University, China. His research interests include manufacturing automation, precision engineering, and signal processing.

LANTAO YANG received the B.S. and M.S. degrees from the Mechanical and Electrical Engineering Department, Shihezi University, China, in 2015 and 2018, respectively. He is currently a Researcher with the State Key Laboratory of Mechanical Transmissions, Chongqing University, Chongqing, China. His research interests include signal processing, gear fault diagnosis, and dynamic modeling of the gear systems.

YIMIN SHAO received the B.S. degree in metallurgical machinery from the University of Science and Technology Beijing, China, in 1992, and the Ph.D. degree in production engineering from Gunma University, Japan, in 1997. From 1997 to 2004, he was a Research Associate with Gunma University and a Visiting Scholar with the EU FP7 Marie Curie International Incoming Fellow, U.K., in 2012. He is currently a Professor and the Vice Director of the State Key Laboratory of Mechanical Transmissions, Chongqing University, Chongqing, China. His research interests include signal processing, noise analysis and pattern recognition, equipment fault diagnosis, intelligent monitoring and residual life prediction technology, precision transmission, and system integration technology.